W.P. Meurer[1], L. Zhao[1], C. O'Reilly[2], S. Daneshgar Asl[3], and I.R. MacDonald[2]

[1] ExxonMobil Upstream Research Company, Spring, TX, 77389, USA

[2] Florida State University Department of Earth, Ocean, and Atmospheric Science, Tallahassee, FL, 32306, USA

[3] University of California, Santa Barbara, Department of Geography, Santa Barbara, CA, 93106, USA

Corresponding author: William P. Meurer (`william.p.meurer@exxonmobil.com`)

Key Points:

- Natural seepage slicks are an expression of oil migration pathways. Oil slicks they create provide a means to understand discharge rates and variability.
- Breaking waves created by higher wind speeds (especially greater than 7 m/s) can rapidly disperse slicks by resuspension of the oil in droplets too small to resurface.
- Combining historical wind speeds with observed slick recurrence rates suggest average slick persistence times of 5 – 6.5 hours in the Gulf of Mexico.

Abstract

Physical processes involved in the ascent of naturally seeped oil from the seafloor and its persistence as a slick are considered. Simplified, physics-based models are developed, drawing in part from the extensive literature concerned with anthropogenic releases of oil at sea. The first model calculates the ascent of oil droplets or oil-coated gas bubbles as they ascend to the sea surface from the seep source. The second model calculates slick longevity as a function of the effect of wind-driven breaking waves. Both models have simplified inputs and algorithms making them suitable for Monte Carlo-type analysis. Using the oil ascent model, we find that slicks from shallower seeps are offset farther relative to their water depth than those from deeper sources. The slick longevity model reveals four growth modes for seepage slicks: persistent (low wind speeds), ephemeral (high wind speeds), reset (all slicks are cleared from an area by high wind speeds), and aging (slick growth after a reset). A year's worth of modeled winds from the Gulf of Mexico indicate average slick ages of ~ 12 hours. Taking account of the expected oil release duration implied by slick recurrences yields average slick longevities for high recurrence seeps of ~6.5 hours and ~ 5 hours for low recurrence seeps. Seep flux estimates that include the length of individual slicks and the constraints of local currents and wind implicitly take into account the impact of wind-speed history. Those that assume a slick age should be re-evaluated in light of the current findings.

Plain Language Summary

Oil is generated in sediment deposited in oceans and seas all around the world. It moves upward because it is lighter than the water in the sediment. Oil that is

not trapped in the reservoirs, like those that provide commercial oil production, can make it to the sea floor and seep into the sea water. When the oil rises to the sea surface it forms slicks that if they are large enough can be imaged by satellites. Repeated satellite images over an area can be used to understand the distribution of sea floor seeps of oil and how much is leaked. This knowledge is fundamental to understanding oil generation and migration processes and the impact of the oil on marine life. Our ability to determine the amount of oil leaking is limited by longevity of the slicks which dictates the likelihood that they will be detected by the satellites. In this study, we develop models to understand how ascent through the water and varying wind conditions impact the formation of and the persistence of natural oil slicks. Our results suggest that previous estimates of slick lifetimes are too long, leading to an underestimate of oil discharge.

1 Introduction

Large pollution releases of oil can have significant impact on marine and near-shore ecosystems. It is therefore important to understand in as much detail as possible aspects of these releases such as the following: dissolution of components in the water during ascent, transfer of hydrocarbons to the atmosphere, and details of the drift of the oil on the sea surface. In contrast, seeped oil occurs in small quantities spread out in both time and space (MacDonald et al, 2015); chemosynthetic ecosystems at seeps may sequester or mineralize a portion of hydrocarbon supply (Johansen et al, 2017). The important aspects to understand about oil seepage, from either the perspective of gaining insight into the ecosystems they support or the hydrocarbon system that feeds them are as follows: the flux of seeped oil, the variability of the flux, the offset of surface slicks relative to the sea floor seepage site, and the persistence of the oil on the water surface.

Considerable effort has been made to understand the ascent and partial dissolution of oil accidentally released during submarine accidents (e.g., blow-outs, pipe-line failures) as it ascends through the water column (e.g., Wei et al, 2009; Socolofsky et al., 2015; Jaggi et al., 2017). A similarly large effort to understand the drift and ultimate fate of large pollution slicks on the sea surface has spanned decades of research (Fay, 1969; Mackay et al., 1980; Lehr et al., 2002; Geng et al., 2016; Brekke et al., 2021; Zhao et al., 2022). Some of the understanding developed in these efforts can be applied to considering the ascent, drift, and longevity of oil released from natural seeps. In both cases oil is being released into the sea from localized sources at the bottom, but the flux rates differ by many orders of magnitude.

A quantitative understanding of how seeped oil migrates to the sea surface and the longevity of natural seepage slicks on the surface is fundamental to understanding seepage as documented via natural seepage slicks. During ascent, oil can be spread laterally by currents causing an increase in its surfacing area and potentially spreading the oil out so much that some or all of it does not form a coherent slick. Once on the surface, the oil can persist for tens of hours as a

slick, or be prevented from ever forming a sizeable slick because of high-energy surface conditions. Knowing how much of the released oil is incorporated into a slick and how long that slick survives on the ocean surface are critical inputs into calculating seeped oil fluxes. Seeps represent the top of oil migration pathways in sedimentary basins, knowledge of fluxes is therefore of practical interest for oil exploration. Understanding the conditions that give rise to long-lived slicks on the sea surface can also be helpful to efforts to sample them (e.g., Wang et al., 2021).

Here we present models suitable for the quantitative understanding of oil migration from seeps to the sea surface and the persistence of natural slicks on the sea surface. We begin our analysis by first considering the extensive literature directed at the many complexities involved in modeling anthropogenic releases of oil at sea (pollution slicks). This section focuses on identifying those physical processes, and to a lesser extent chemical processes, that natural seepage and anthropogenic oil releases have in common. Using insights gained from the pollution modeling literature, we develop a simplified model that focuses on the key physical processes involved in the generation of natural seepage slicks. Basic chemistry is included as required for the physics. Our focus on physical processes is motivated by their relative importance (discussed below) and because the chemical contributions from seeped oil are not a significant contribution to the oceans or atmosphere.

2 Background

Models to assess the impact of anthropogenic releases of crude oil or refined petroleum products have been around for decades (Keramea et al.; 2021). Most efforts for understanding the fate of oil released into the sea have focused on high flux pollution events (e.g., well blow-outs, pipe-line failures, tanker and ship fuel tank ruptures) because of the environmental and social costs of these large releases. Some of this work can be applied directly to understanding natural releases of crude oil or at least provide insights into important processes. Here we briefly consider aspects relevant for understanding natural seepage processes. These models consider oil release and transport from sea floor sources, transport and degradation on the water surface, or both. We consider water column processes first and then those on the sea surface.

Understanding the release of pressurized oil from a well blow-out or pipeline leak requires knowledge of processes related to initial jet momentum and dynamics, and plume buoyancy (Sim et al., 2015; Lehr and Socolofsky, 2020). The release rates at natural seeps are too small to make many of these processes relevant. However, physical models concerned with buoyant ascent of discrete droplets can be generally applied to understanding natural seepage processes. For dispersed oil droplets and oil-coated gas bubbles, knowledge of the velocity structure of the water column and the size distribution of the particles is most critical (Yapa et al., 2012; Zhao et al., 2014; Pesch et al., 2020). The TAMOC model includes options to track the behavior of single fluid particles (oil droplets or gas bubbles) or a group of various size particles (Dissanayake, et al. 2018; Gros et al., 2017).

This model has been used to track oil droplets from natural oil seeps (e.g., Razaz et al, 2020).

Chemical processes at subsea oil releases share considerable similarity between anthropogenic releases and natural seepage. In both systems, the main chemical processes involve diffusive exchange of components between the oil and water and the impacts of changing pressure and temperature on the oil during ascent (Gros et al., 2017). The main initial chemical difference between anthropogenic and natural releases of oil is found in the fraction of light hydrocarbons found in the oil. Blow-outs allow crude oil under high pressure to ascend rapidly to the surface. They are out of equilibrium with the sea floor temperature and pressure and contain excess light components, such as methane, that are rapidly lost from the oil. Conversely, oil released from a leaking pipeline or sunken tanker has likely been stripped of most of its more volatile light components during extraction and processing. Oil from natural seeps falls between these extremes containing some lighter hydrocarbon components as would be expected for oil equilibrated at the pressure and temperature of the seep.

Physical processes impacting oil at the sea surface mainly affect its transport, either along the sea surface or in/out of the water column (Simecek-Beatty and Lehr; 2017). The impact of wind speed on the dispersion of pollution oil slicks has received both experimental and theoretical analysis (De Dominicis et al., 2016). For the purposes of understanding their longevity, the main distinction between most pollution and natural seepage slicks is the average thickness of the oil layer. Significant pollution slicks can have thicknesses measured on the scale of millimeters (Zatsepa et al., 2018). Seepage slicks have average thicknesses that are less than a micron which is demonstrated by the slick coloration ranging from rainbow to silver sheen corresponding to thickness of ~1 to 0.1 microns (e.g., Allen et al., 1970; MacDonald et al., 1993). This means that the oil droplet sizes generated when breaking waves force a surface layer of oil into the water column are large enough to resurface for pollution slicks but not for seepage slicks (Tkalich and Chan, 2002; Zatsepa et al., 2018). Zatsepa et al. (2018) combined experimental and theoretical analyses to determine that oil in slicks with a layer thickness of less than ~10 m will be lost to resuspension during breaking wave events. Another physical process that removes oil from the sea surface involves adhesion of oil to particles such as marine snow that ultimately sink (Li et al, 2020). Relative to the potential immediacy of breaking waves on seepage slicks, loss of oil as marine snow requires much more time and is important in low wind speed environments.

Chemical processes on the sea surface impact the longevity of oil slicks on a range of time scales. Volatilization of lighter hydrocarbons can take place relatively rapidly from a thin layer of oil with nearly complete loss of the C_{17} components within 12 minutes of surfacing (MacDonald et al., 2002; Gros et al., 2020). Dissolution of components may be important for surface spills but substantially less so for oil released at depth since it will have already lost its most soluble components during ascent through the water column. Other chemical processes

such as photo-oxidation (Aeppli et al., 2022) and biodegradation (e.g., Xue et al., 2015) are important at time scales of a day or more.

3 Oil Ascent and Slick Longevity Models

Two separate sets of algorithms were developed to understand the fate of oil released from natural seepage sites. The first focuses on the transit of oil droplets and oil-coated gas bubbles through the water column. The second examines the persistence of natural seepage slicks on the sea surface.

The behavior of hydrocarbon particles (oil droplets or oil-coated gas bubbles) in the water column is considered using three co-dependent attributes. We assess the rise velocity by considering (1) how the particles interact with the water, (2) lateral spreading of particles using a modified random walk algorithm, and (3) the physical characteristics of the particles as governed by pressure, temperature, and composition using a black-oil correlation.

The longevity of seepage slicks on the sea surface is extremely sensitive to the wind speed – especially at speeds greater than ~ 5.5 m/s. We use an empirical correlation between wind speed and white-cap coverage area to estimate the area impacted by breaking waves as a function of wind speed. We then use a probabilistic model to calculate the rate of loss of a natural slick over time as a function of the breaking wave area. In the model, slick loss occurs as holes (oil free patches) corresponding to the area of the breaking wave within the area of the slick.

3.1 Ascent of Oil through the Water Column

The ascent of oil through the water column and its ultimate surfacing is calculated using a modified random walk particle tracking approach adopted to track the movement of fluid particles. The model uses the water column horizontal velocity field as the primary input in determining the lateral displacement of particles. The speed of ascent of the particles determines how long they are in the water column and therefore how far they can be displaced.

The ascent speed of oil droplets and oil-coated gas bubbles depends on the size and shape of the particles. Particle shapes are determined, in part, by the particle size. If a particle's diameter is less than 1.0 mm, it has an essentially spherical shape. Stokes law is adequate for determining the rise speed of such small spherical particles, but not for large ones. For particle sizes larger than ~1.0 mm but less than a critical diameter d_{cr} (herein equal to approximately to 10.0 mm), the particle takes the shape of an ellipsoid. For particles of size larger than d_{cr} (normally bubbles), the shape of the particles is a spherical cap (see figure 2.4 of Clift et al., 1978). We use empirical relations reported by Clift et al. (1978) and Zheng and Yapa (2000) to estimation the rising velocity of a particle based on their diameters such that:

1. Small spherical shape (d 1 mm):

$$W_p = \frac{R_e \mu}{\rho_c d} \quad (1)$$

where is the dynamic viscosity of the continuous phase (Pa s) (i.e., water herein); $_{c}$ is the density of the continuous phase (kg/m^3); d is the particle diameter (m); Re is the Reynolds number computed according to Clift et al. (1978).

1. Ellipsoidal shape (1 mm < d_e d_{cr})

$$W_p = \frac{}{\rho_c d_e} \mathrm{Mo}^{-0.149}(J - 0.857) \quad (2)$$

where d_e is the equivalent diameter (m), d_{cr} is the critical diameter between ellipsoidal shape and spherical cap shape; J is a general correlation which can be expressed as:

$$J = 0.94H^{0.757} \qquad (2 < H \leq 59.3) \quad (3a)$$

$$J = 3.42H^{0.441} \qquad (H > 59.3) \quad (3b)$$

in which the term H is given by:

$$H = \frac{4}{3}\mathrm{EoMo}^{-0.149}\left(\frac{\mu}{\mu_w}\right)^{-0.14} \quad (4)$$

where $_{w}$ is dynamic viscosity of water in Braida's experiments (Grace et al., 1976), taken as 0.9 cp, the term *Eo* is the Eotvos number, and *Mo* is the Morton number, both reflect the shape of the particle, and are defined as:

$$Eo = g\ \rho d_e^2/\sigma \quad (5)$$

$$Mo = \frac{g\mu^4\rho}{\rho_c^2\sigma^3} \quad (6)$$

The Eotvos number is a dimensionless number that represents the ratio of buoyancy forces to interfacial forces, and the Morton number represents the ratio of forces deforming the droplet to those keeping it spherical.

1. Spherical cap shape ($d_e > d_{cr}$)

$$W_p = 0.711\sqrt{g d_e\ \rho/\rho_c} \quad (7)$$

The size of oil droplets and oil-coated gas bubbles from seeps are generally less than 10 mm (d_{cr}) at release depth (e.g., Johansen et al, 2017). However, as bubbles ascend, gas expansion due to pressure drop may cause the size of bubbles to exceed d_{cr}. The critical diameter d_{cr} of the transition from ellipsoidal to spherical cap shape can be determined empirically by solving Eq. 2 and 7 simultaneously to get the intersection point.

Given the ascent speed, we use a modified random walk particle tracking approach to track the movement of fluid particles. The fluid particles, oil droplets or oil-coated bubbles, are grouped into multiple volume bins. Ascent behavior of particles within a given bin are calculated based on the mean volume of each bin. The particle movement during ascent determines when and where each particle emerges on the sea surface.

Particle tracking was performed on the designated particle volume for each bin to estimate their rising trajectories (oil droplets and oil-coated gas bubbles) in the

water column. This combines the rising velocity of particles and ocean horizontal current and turbulent diffusion at designated depths. Vertical ocean current and diffusion have lesser impacts on particle movement (mostly generating scatter around the mean); thus, they are not considered here. The offset from the source over depths is given as:

$$x_{i,\ pj} = x_{i-1,pj} + U_i\ t + R\sqrt{2D_x\ t_{i,\ pj}} \quad (8)$$

$$y_{i,\ pj} = y_{i-1,pj} + V_i\ t + R\sqrt{2D_y\ t_{i,pj}} \quad (9)$$

where x and y represent the horizontal distance (m) to the source in the east and north directions, respectively; the subscript i represents the location at the designated depth, where x_0=0 is the seep location at sea bed and the calculation was from bottom up; the subscript pj represents the location of a particle size j; U and V are the velocity components of ocean current (m/s); R is a random number with mean 0 and variance 1; D_x and D_y are the turbulent diffusivities (m^2/s) in the x and y directions (the values of subsurface D_x and D_y in the ocean waters are normally low, ~0.1 m^2/s); t is the time step (s) with,

$$t = \frac{h_i}{W_{pi,pj}} \quad (10)$$

for any given depth interval h_i (m), and W is the rising velocity (m/s) (discussed later) for a particle size j within h_i.

An example of the trajectories of various sizes of oil droplets under a typical medium energy ocean current reveals that droplets with size > ~2 mm are grouped together on the surface (Fig. 1). Droplets within this size range typically contain the majority of oil mass that reaches the surface sufficiently close together to form surface slicks potentially large enough to be captured by the radar.

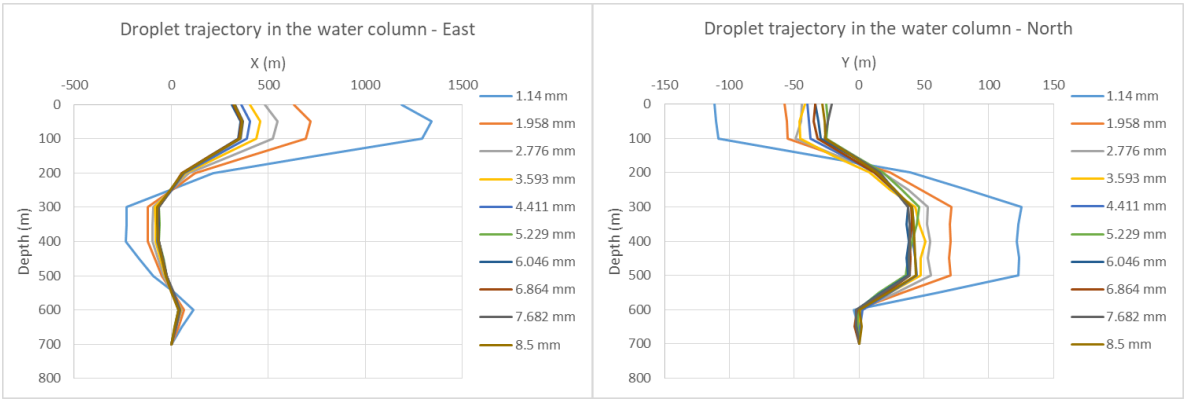

Fig. 1 Rising trajectories of oil droplets under a typical medium energy ocean current. Droplets were grouped into 10 size bins. Note droplets with size>~2 mm are lumped together on the surface.

The impact of changing pressure and temperature during ascent of hydrocar-

bons in the water column changes the physical properties of the oil and its relative saturation of methane. We use a black-oil correlation (McCain, 1991) to estimate the physical properties of the oil and gas as a function of pressure and temperature. The correlation requires an estimate of the API gravity of the oil and initial methane saturation of the oil as compositional inputs. It can also be used to calculate the expected saturation of the oil in a methane-rich gas phase.

The water solubility of most hydrocarbons with more than five carbons is extremely limited so they are mostly retained in oil during its ascent. An exception to this are the relatively soluble BTEX compounds (Benzene, Toluene, Ethyl-Benzene, and the Xylenes), but these account for a modest volume fraction of most crude oils. This limited solubility does not significantly impact the physical properties of the oil during ascent.

The presence of a separate gas phase in an oil droplet, generated by methane ebullition, could significantly decrease its density. However, methane diffusion between a hydrocarbon gas bubble and sea water is relatively rapid (Rehder et al., 2009). Since any gas bubbles are likely to nucleate at the boundary between the oil and the water, as this would minimize the free-energy of nucleation, any bubble growth would be substantially or completely retarded contributing negligible buoyancy. This interpretation is consistent with laboratory experiments (Pesch et al., 2018) and equation-of-state thermodynamic modeling that predicts that no discrete gas phase would be present until relatively near the sea surface (Gros et al, 2020). We therefore assume that the ascent speed of rising oil droplets is not significantly impacted by the ebullition of methane.

The ascent of oil-coated gas bubbles is governed, in part, by the rate of gas loss from the bubble. Observations suggest that clean gas bubbles dissolve after ~100 m of vertical ascent when starting in water depths of 200 m or more (e.g., Rehder et al., 2009); whereas, oil-coated gas bubbles have been observed to ascend from depths as great as 3400 m to the sea surface (Römer 2019). For oil-coated bubbles, the oil film around the gas bubble does not stop gas dissolution, but requires a two-step process: the gas is first partitioned between the gas and the oil coating and then partitioned between the oil and the surrounding water through the oil-water interface. Note that this process also limits the ability of dissolved gases in the water from transferring to the bubble as their rate of transfer will be severely limited by their partitioning into the oil coating. There are very limited studies on the transfer of gas from oil-coated bubbles; however, the dissolution rate is clearly slower than for uncoated bubbles. As an approximation, we suggest the dissolution rate might be similar to the situation where a hydrate shell is present. This implies a reduction of dissolution rate by a factor of 5 (Rehder et al., 2002, 2009) compared to the rate of uncoated bubbles.

To calculate the mass loss of gas from ascending bubbles we first calculate the mass transfer, m_{diss}, for a given pressure and temperature and then apply the factor of 5 correction.

$$m_{\text{diss}} = -K_{\text{cb}} A \left[S_{\text{solubility}} - S_0 \right] \quad (11)$$

where K_{cb} is the mass transfer coefficient; A is the surface area of the coated bubble; $S_{solubility}$ is the solubility of a gas component; and S_0 is the ambient concentration of the component. The mass transfer coefficient K_{cb} for dirty bubbles is estimated based on the formulation developed by Zhao et al. (2016):

For d 0.4 mm, $K_{\text{cb}} = 0.552 Re^{1/2} \left(\frac{v}{D}\right)^{1/3} \left(\frac{D}{d}\right)$ (12a)

For 0.4 mm < d 5 mm, $K_{\text{cb}} = \frac{2}{\sqrt{\pi}} \left[\left(1 - \frac{2.89}{\sqrt{\text{Re}}}\right) \frac{D W_b f_R}{d} \right]$ (12b)

For d > 5 mm, $\frac{K_{\text{cb}}}{D^{1/2}} = 4.5 \left(\frac{1}{0.45 + 0.03d}\right)^{1/2}$ (12c)

where D is molecular diffusivity of the substance in liquid (cm^2/s); *Re* is bubble Reynolds number $Re = \frac{dW_b}{v}$, and v is the kinematic viscosity of the liquid (m^2/s). f_R is a correction factor for the extent of the interfacial immobility by the deposition of surfactant, and can be expressed as (Tsuchiya et al., 1997). For methane-rich bubbles, the above correlations can be simplified (Fig. 2) such that: if d 0.4 mm then K=0.002, if d > 5 mm then K=0.008, if 0.4 mm < d 5 mm then K=$-2.2 \times 10^{-5} + 0.1119\text{d} - 32.604\text{d}^2 + 2878.5\text{d}^3$.

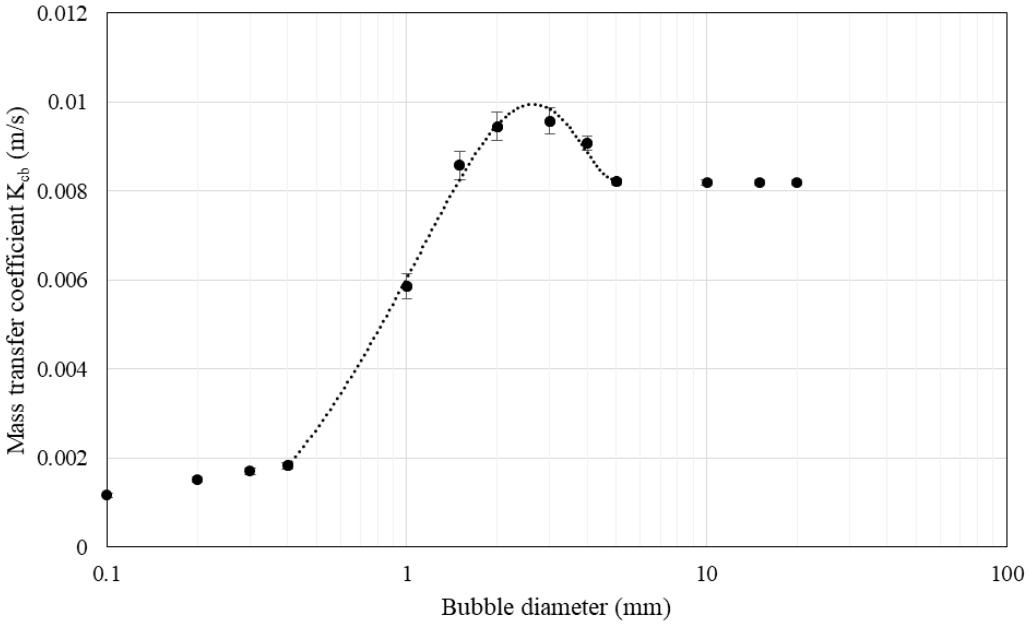

Fig. 2 Mass transfer coefficient K for methane-rich dirty bubbles.

3.2 Persistence of Slicks on the Sea Surface

Crude oil reaching the sea surface from a natural seep undergoes a variety of processes. As the oil droplets or oil-coated gas bubbles reach the surface, the oil

quickly undergoes gravitational collapse and rapidly spreads to a micron or submicron thickness layer (often referred to as sheen) by the surface tension forces (Fay, 1969). Seen from close proximity, this spreading creates a round "pancake" of oil with color variations that reflect the changes in thickness from the site of surfacing to the leading edge of the spreading sheen (Fig. 3). Pancakes formed in close proximity coalesce to form large slicks that are progressively displaced from the oil surfacing origin (OSO) by wind and surface currents.

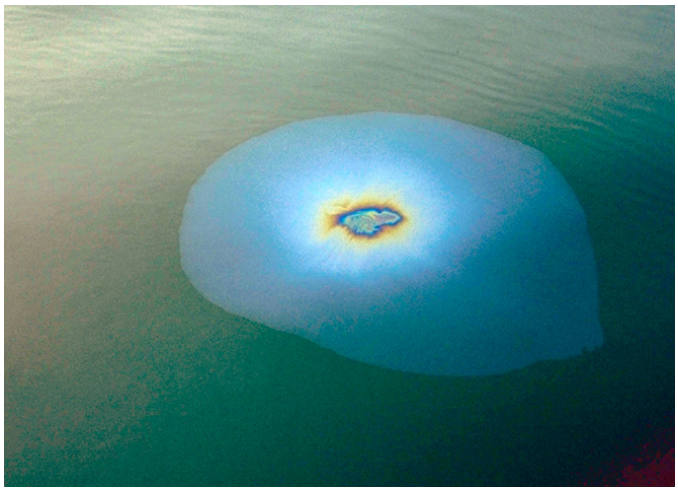

Fig. 3 Photograph of a recently surfaced oil droplet. The color variations correspond to destructive and constructive refraction of visible light as the spreading layer thins from ~5 to 0.4 μm. Thinner layers may noticeably reduce surface roughness, but are otherwise invisible.

Experimental and theoretical work have demonstrated that when oil in a seepage slick is forced into the water by breaking waves, it forms droplets that are too small to resurface (Tkalich and Chan, 2002; Zatsepa et al., 2018). Hence, having a robust approach to calculating the area of breaking waves as a function of wind speed is essential. Theoretical estimates of breaking wave areas and/or sea surface turn-over ratios either assume a fully developed sea (wave heights and periods correspond to that expected for the observed wind speed for unlimited fetch) or apply a correction to account for a partial approach to a fully developed sea (e.g., Tkalich and Chan, 2002). We have opted for a more empirical approach to estimating the breaking wave area using the white cap coverage produced by breaking waves.

Although some wave breaking occurs at lower wind speeds (Phillips, 1985), most wave breaking is associated with wind speeds capable of whitecap formation. Therefore the whitecap coverage (WCC) can be viewed as being proportional to the area of wave breaking as a function of wind speed.

The relationship between WCC and wind speed as measured 10 m above the sea surface (U_{10}) has been empirically calibrated (Callaghan et al., 2008). The

relationship (Eq. 13) is split at U_{10} ~11.25 m/s because, at speeds higher than this, shearing of the wave tops occurs.

$$WCC = 3.18x10^{-3}(U_{10} - 3.70)^3; 3.70 < U_{10} \leq 11.25 \quad (13)$$

The slick area loss caused by breaking waves (S_{LW}) can be calculated from the WCC as a fractional area (Eq. 14). The time associated with wave breaking is governed by the wave period (T_m).

$$S_{LW} \approx \frac{WCC}{T_m} \quad (14)$$

To convert Eq. 14 into an equality, a time step must be used that is necessarily shorter than the time required to reach an equilibrium wave height at a constant wind speed, but long relative to T_m. A time step that allows a reasonable approach to equilibrium given a dynamic initial state is best (e.g., 30 minutes in Eq. 15) and we suggest not using time steps shorter than ~10 minutes. The time step is multiplied by the WCC to account for the correct number of wave periods. The percent WCC is converted to a fractional area by dividing by 100. To complete the equality the WCC must be corrected for the fact that it does not map directly to the breaking wave coverage. We use a scaling coefficient ( ) to account for: the larger size of the whitecap area relative to the breaking wave area and the persistence of whitecaps after wave breaking (captured in the imagery used to construct the correlation). The exact value of is not known and likely has some dependence on wind speed. Reasonable estimates can be made from the study of whitecap formation and persistence (e.g., Callaghan et al., 2012). Likely bounds for the factors that contribute to are: WCC ~ 1.5 to 2.5 times larger than breaking wave area and ~1 to 2.5 seconds for the persistence of the whitecaps after initial wave breaking. This suggests that should be bounded between 1.5 and 6.25. Note that if the WCC were taken directly as a measure of the breaking wave area this would be equivalent to setting equal to one in Eq. 15.

$$S_{LW}^{30min} = \frac{WCC}{T_m} \frac{(1800 \text{ s})}{(100 \bullet \beta)} \quad (15)$$

The value of has a significant impact on the rate the wind causes slick destruction, especially at higher wind speeds (Fig. 4). The empirical observations of the impact of wind speed on slick persistence suggest that at speeds greater than ~7 m/s slicks undergo rapid degradation (Daneshgar Asl et al., 2017). These observations suggest the value of should give appreciable slick degradation at wind speeds at and greater than 7 m/s. We have used an intermediate value of = 4. This choice is evaluated using observational data as there are currently no experimental data for calibration.

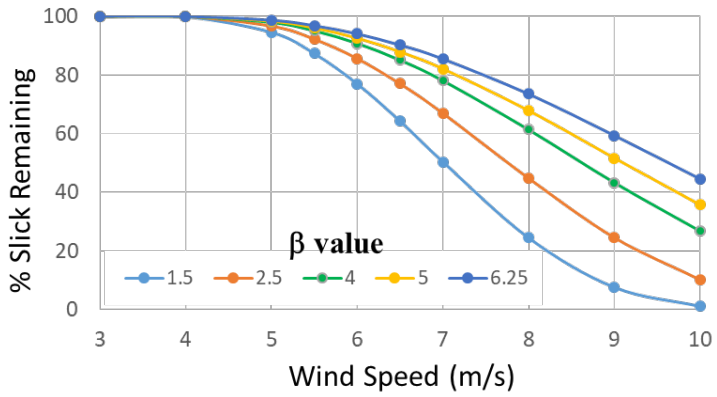

Figure 4 - Impact of scaling coefficient ( ) on the calculated percent area loss from a slick as a function of wind speed after one hour exposure. Calculated using Eq. 4 modified for a 10 minute time step.

The calculation for slick area reduction can be simplified by fitting a polynomial to the solutions to the equations across a range of wind speeds (Eq. 16). One polynomial solution is used for wind speeds < 4 m/s (limited breaking waves) and another for speeds 4 m/s. The solution to Eq. 16 yields the fractional area lost (Loss) from a slick for a 30 minute time step (recommended) as a function of wind speed (WS); it needs to be multiplied by the percentage of the slick area remaining in the preceding time step to calculate the percentage of the slick area lost.

$$\text{Loss} = 0.0000462384*\text{WS}^2 - 0.0000003354*\text{WS} + 0.0000000550 \quad (16a)$$

$$\text{Loss} = 0.0000088923*\text{WS}^5 - 0.0003704257*\text{WS}^4 + 0.0063128253*\text{WS}^3$$

$$- 0.0415516340*\text{WS}^2 + 0.1136208513*\text{WS} - 0.1070759664 \quad (16b)$$

In solving Eq. 16 the bounding calculation for the initial surfacing of the oil is different from the ongoing calculation for oil already on the sea surface. During the initial surfacing of the oil, we assume continuous release over the time step. This creates a condition such that oil released at the very start of the time step sees the full duration but oil released at the very end of the time step sees virtually no impact from waves. To account for this, we reduce the impact of the wind on the oil slick by 50% for this initial boundary time step. After the initial time step. all the oil for that batch is on the surface, but an adjustment needs to be made to the wind impact to account for the fractional slick area loss in preceding time steps. The logic here is that as the slick ages, the breaking waves will create discontinuities (holes) in the slick and some fraction of future waves breaking inside the slick perimeter will partially or wholly impact these discontinuities reducing the rate of slick loss. This adjustment of the wind impact as a function of the area of the slick can be seen looking at a time series of the results for various wind speeds (Fig. 5).

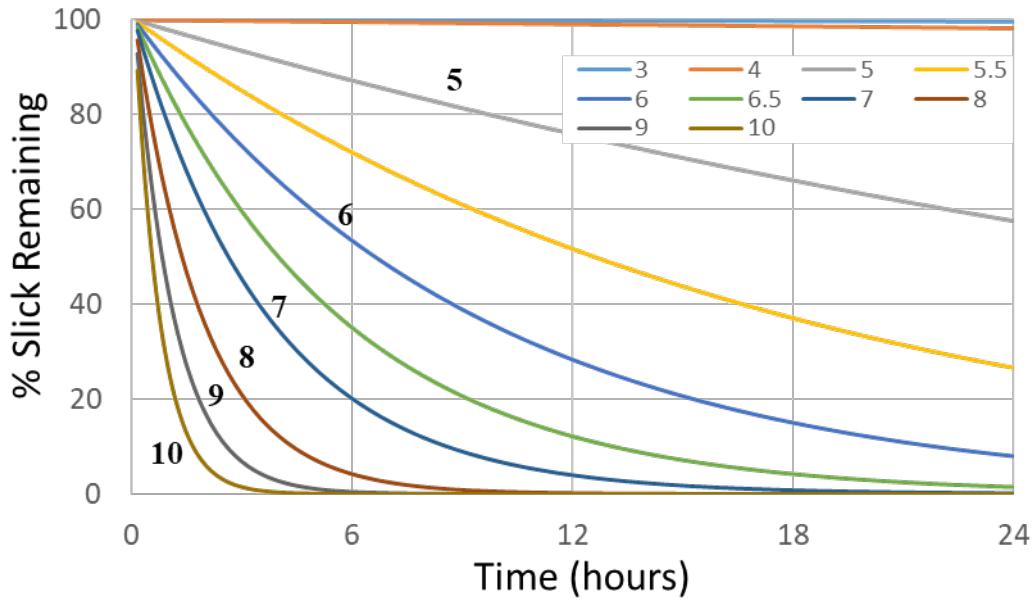

Figure 5 – Percentage slick loss is shown as a function of time and wind speed. Wind speeds curves are color coded (see legend) and curves for 5, 6, 7, 8, 9, and 10 m/s are labeled for additional clarity.

The processes of slick destruction via breaking waves has a negative feedback. At high wind speeds ($>$ 7 m/s) the slick is lost very rapidly. The loss curves asymptotically approach zero as the fraction of the original slick area becomes small and the probability that a breaking wave will impact the remaining slick diminishes. At lower wind speeds (5 m/s) the loss curves look linear over a 24 hour period because little area is lost to create a negative feedback. Intermediate curves shallow as time progresses and the amount of slick lost becomes a significant factor in the calculation.

4 Results and Discussion

We begin our discussion by considering model validation and performance based both on the fit to observations/experiments and limitations imposed by the inputs to the models. With an understanding of the limitations of the models we then use the oil ascent model to evaluate the offset of oil surfacing origins (OSOs) in different water depths and ocean current structures. The slick longevity model is used to better understand how wind speed variability impacts slick persistence. Lastly, we use the model to consider how slick longevity influences estimates of seepage flux.

4.1 Model Validation and Performance

Comparison of model predictions for bubble and oil droplet ascent velocities with experimental and empirical observations is a straightforward way to gain confidence in the model. The ascent speed of oil and gas bubbles through water has seen considerable study and can be readily compared to the model results. We found no data that explicitly tabulates the age of seepage slicks on the surface as a function of wind speed. For this comparison we use data collected as part of the study of the seeps in the GC-600 lease block in the Gulf of Mexico (Daneshgar-Asl et al., 2017).

To validate the hydrocarbon particle ascent model based on Equations 1-7, three cases were computed and compared with experimental data (Fig. 6). These include single oil droplets in fresh water, single air bubbles in fresh water, and hydrate-coated gas bubbles in sea water. The predicted rising velocities for these cases show good agreement with measurements. The rising velocity W_p increases with particle size for d<3 mm due to the increased buoyancy forces as particle size increases. Then W_p starts to slightly decrease with particle size. This is because some of the energy from the buoyant rise is transformed into horizontal oscillatory motions due to the shape changes. Finally, at sizes larger than d_{cr}, the horizontal oscillations decrease, and the buoyancy force dominates the particle rising movement again.

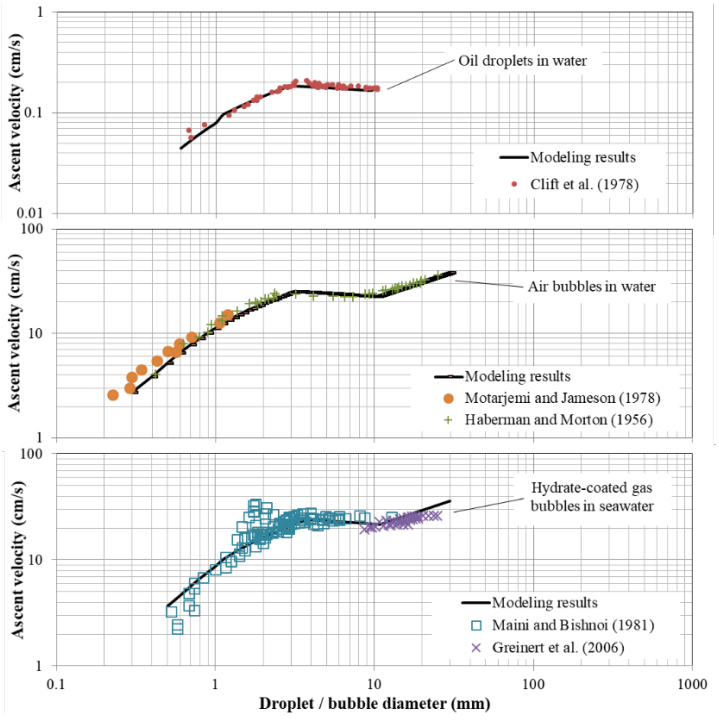

Figure 6 - Comparison of the predicted rising velocities to the experiment measurements from literatures: a) Oil droplets in water; b) air bubbles in water; c)

hydrate-coated gas bubbles in seawater.

Our understanding of the physics and chemistry involved in the ascent of oil through the water column likely exceeds our knowledge of the current structure and particle size distribution appropriate for any particular application. The current structure of the water column varies on different time-scales as a function of depth, with shallow currents being the most variable on shorter time-scales. Uncertainty in the water column velocities can introduce variations in OSO locations of a kilometer or more, depending on water depth (see results below). The distribution of droplet or oil-coated bubble sizes can also shift the projected location of an OSO. Size distributions can vary with flux and likely also vary based on the very local character of the sediment where the oil is being released. The impact of this size variation is mostly on the area of the OSO as the bulk of the oil is likely to be in the bubble size range that ascends at similar rates (Fig. 6).

Validation of the surface persistence model is problematic because it ideally requires a dataset that tracks evolution of multiple slicks, with wind speed measurements taken along the slick lengths as they spread. To our knowledge, this detailed data has not been collected for a single slick, much less a statistically large number of them. The hindcast modeling approach presented by Daneshgar-Asl et al. (2017) required a dataset that provides a fair substitute. It is based on a single synthetic aperture radar (SAR) image of a slick with the OSO identified. Hindcast wind and surface current data are used to calculate the expected trajectory of the slick from its OSO to its end point, iterating until the observed offset between these points is approximately matched by the calculated offset. One of the products of the hindcast model is an estimation of the age of the slick (i.e., how long did it take to spread the observed distance from the OSO). The modeling data includes the average wind speed over the entire length of the slick for its entire drift history. We can thus use the observed slick-age and wind-speed relations from the data analyzed by Daneshgar-Asl et al. (2017) to compare to the slick persistence model as a function of wind speed (Fig. 7). The slick data show general agreement with the model curve. However, there is scatter about the model curve especially at lower wind speeds.

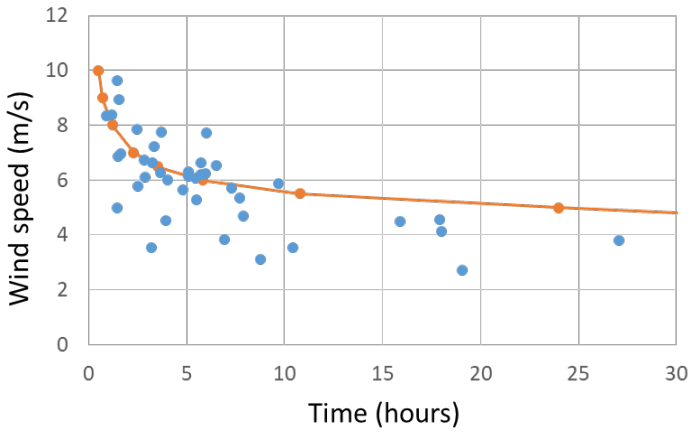

Figure 7 – Comparison of slick ages as a function of wind speed for slicks originating in the GC-600 lease block in the Gulf of Mexico (blue circles) with the slick persistence model (orange circle connected with solid line).

The model curve defines the time it takes for an area with 100% oil coverage to be degraded to 55% oil coverage. As the slick is degraded, the image captured by a SAR satellite has progressively lower contrast and more diffuse boundaries. Both of these are critical to identification of slicks. The choice of 55% coverage as the detection threshold is arbitrary but seems like a reasonable criteria. Re-calculation of the model curve to higher or lower residual coverages shifts the curve with larger changes for lower wind speeds and smaller changes for higher wind speeds. In the discussion below, we assume detection of slicks via SAR imagery and use the 55% remaining coverage as the detection threshold.

The scatter of points around the model curve (Fig. 7) reflects the divergence of the observations from the assumption of constant wind speed and should be expected. This is because the model curve represents slick ages for oil released in a constant wind-speed environment. For example, the model predicts that at a constant wind speed of 6 m/s a natural slick will no longer be detected by SAR in ~6 hours and at 5 m/s wind speed it persist for ~22.5 hours. For a constant release of oil from a seep under constant wind speeds the observed slick length should plot along the model curve. However, if the preceding wind speeds were higher or the release of oil from the seep started less than 6 or 22.5 hours ago, then the slick length should fall to the left and below the model curve. In contrast, points to the right and above the model curve (Fig. 7) are explained by sharp increases in the wind speed after a period of low wind speed. During a low wind-speed period substantial oil can accumulate on the water surface. As wind speeds increase, there is a lag in the destruction of the slick relative to the current wind speed.

The importance of the wind-speed history on the slick age can be modeled using buoy wind-speed data from the Gulf of Mexico (data details are discussed

below). We used the wind-speed history to calculate expected slick ages for an entire year at 10 minute time steps and compared it to the model curve for equilibrium slick lengths (Fig. 8). As with the observational data from GC600, the model ages scatter above and below the model curve. One take-away from this analysis is that the wind-speed history needs to be integrated into any evaluation of the slick persistence model. However, the general conformance of the observational data from GC600 with the modeled ages using actual wind-speed history, suggests that the model fairly predicts the impact of the wind on seepage slicks.

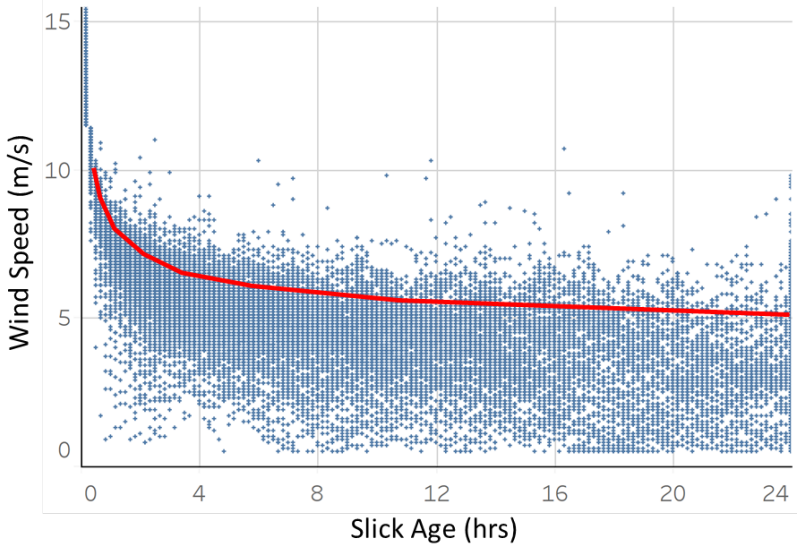

Figure 8 – Comparison of modeled slick ages generated from a continuous wind-speed record (diamonds) with the slick persistence model (red solid line). The model restricted the maximum slick age to 24 hours (see text for details).

4.2 Evaluation of OSO Offset from Seep

The oil ascent model allows for rapid Monte Carlo predictions of the location of OSOs from a seep source (or vice versa) given a model of the water column velocity structure. The model can be used to predict assuming oil droplets only, oil-coated gas bubbles only, or both droplets and bubbles. For example, ADCP profiles of the water column above the Bush Hill seep, north-central Gulf of Mexico (Meurer et al., 2021), can be used to model the expected OSO locations for the time period represented by the data (Figure 9A, 9B). The spread of model OSOs uses the bounding ADCP profiles for each day and allows a 35% correlated, relative standard deviation for the Monte Carlo simulations. These data allow for discriminating the likelihood that slicks observed in the Bush Hill area can be ascribed to Bush Hill as opposed to other seeps. Where detailed current data is not available, hindcast ocean models such as the HYbrid Coordinate Ocean Model (HYCOM) (Bleck, 2002) can be used as model input. Examples

for potential seepage sites offshore Namibia and Mauritania were modeled using a year's worth of current data with the observed variability of the data used for the Monte Carlo simulations (Figure 9C, 9D). In all cases the offset for oil-coated gas bubbles is less than for oil droplets.

For the set of examples modeled here, the average offset of the OSO increases with greater water depths. However, this need not be the case. Seepage sites in shallower water where current focusing results in higher speed currents can result in greater OSO displacement than in deeper water. This result has been observed in the relative OSO offset in Congo Basin where some slicks originating from deeper sources show less offset than those from shallower sources (Jatiault et al., 2018).

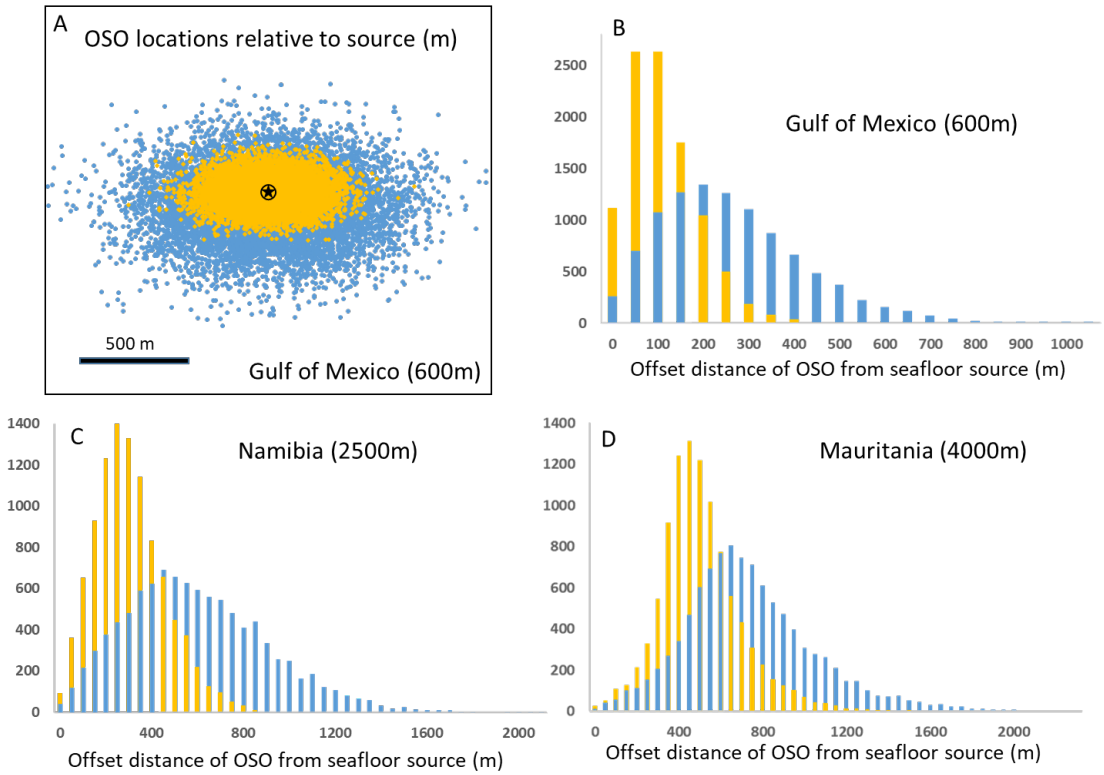

Figure 9 – Shown are the results of 10k Monte Carlo simulations of OSO locations for seeps located in differing locations and water depths (see text for model details). In all examples OSO generated by the surfacing of oil-coated bubbles are in yellow and those for oil droplets are in blue. (A) Predicted OSO locations for slicks from a ~600m deep source in the north-central Gulf of Mexico relative to the seafloor source (star symbol). Histograms of OSO offsets from the source position in (B) 600m in the Gulf of Mexico, (C) 2500m offshore Namibia, (D)

4000m offshore Mauritania.

Simulations of OSO distributions can provide a basis for distinguishing the presence of multiple seepage locations. This is especially useful for distinguishing seepage sites in places with abundant seepage such as the northern Gulf of Mexico. Garcia-Pineda et al. (2010) proposed a simple linear relationship for the expected maximum offset of OSOs in the Gulf of Mexico. Analysis of hindcast water column velocity profiles from across the area could be used to test this rule of thumb. In areas with more sparse seepage, models of OSO offset can be used to assess the likelihood that spatially clustered slicks are repeat features from the same seepage point. This is important for defining seepage locations for sampling slicks (e.g., Wang et al., 2021) or for gaining confidence that SAR interpretations that features are natural seepage slicks actually are.

Although the examples presented here (Fig. 9) are forward-modeled distributions of OSOs from a known source's location, the model can be used to invert OSO locations to model potential source locations. When used this way the OSO location is used as the starting location and a population of current structures are used to backtrack the droplets/bubbles to a distribution of source locations. Overlap of results from multiple OSOs should provide a means of triangulating the source location.

Najoui et al., (2018) developed a method for backtracking seep source locations from OSOs based on a simplified physics model for ascent velocity (Goncharov, 2009) that they applied to the Gulf of Mexico. The model backtracks the ascent paths for different droplet sizes for each OSO and identifies source locations by the locations where paths from multiple OSOs cross. The technique yields an average OSO offset of ~2500 m for 242 seep sources that are not differentiated by water depth. The model also predicts some offset distances greater than 17 km, significantly greater than any predicted using the oil ascent model presented here.

4.3 Significance of Slick Longevity

Detection of natural seepage slicks at the sea surface is determined by two factors, (1) the release of a sufficient quantity of oil for enough time to allow a detectable slick to form and (2) the ability of the resulting slick to survive on the sea surface long enough to be imaged. Both of these factors depend upon the method for detecting or imaging the slick. For example, observation of surfacing oil droplets from a ship on location requires only drops of oil to make it to the surface and to survive for long enough for an observer to spot them. In contrast, satellite detection requires a feature with at least 100 to 150 pixels worth of area; the amount of oil depends strongly on the resolution of the image. Assuming a uniform thickness of 0.1 m, pixel sizes of 10, 25, and 100 m require 1.5, 6.25, and 150 l of oil, respectively, to create a 150 pixel slick. Fluctuations in the rate of supply of oil and/or more/less rapid destruction of a slick can cause the area covered by an oil slick to vary above and below the detection threshold. The question of detection then is framed as a probability

that a satellite will image the area of the slick when the slick's area is above the detection threshold. Slick longevity and oil flux are thus the main controls on observing slicks. The longer the oil persists on the sea surface the lower the oil flux required to generate a detectable slick and conversely the more oil being supplied to the sea surface per unit time the shorter the slick longevity that is required to maintain a size large enough to be imaged.

Analysis of seepage slicks from basins around the world suggest that the largest and longest slicks occur after extended periods of low wind speed (Garcia-Pineda et al., 2016; Jatiault et al, 2017). The slick persistence model can be used to examine expected variations in slick ages for a given wind-speed history. To do this we analyzed a year's worth of data (Jan 1 2000 – Dec 31 2000) from a moored NOAA buoy (Station 42041, 27.504N 90.462W) from the central Gulf of Mexico. The buoy collected average wind velocities binned into 10 minute intervals. The dataset for the year is nearly complete, with only 78 missing values out of 52,704. Missing values were extrapolated using a linear interpolation to create a continuous record. Based on the wind-speed history the age of slicks in this area can be modeled throughout the year (Fig. 10). The model assumes that a seep is always active and always releasing enough oil to be detected. This means that a slick that is 10 minutes old is always present. We set the maximum slick age to 24 hours based on the recognition that the model only examines the role of the wind in degrading slicks and at longer times the cumulative effects of other processes (e.g., photo-oxidation, flocculation as marine snow, biodegradation, etc.) will be important in determining slick longevity.

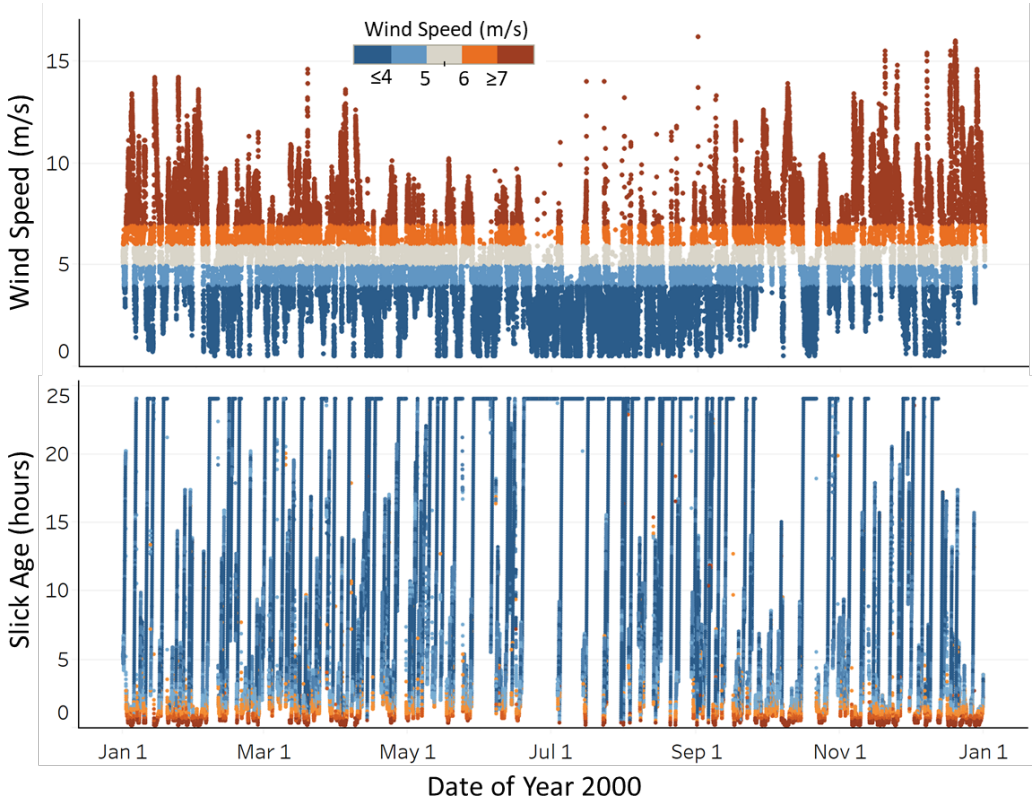

Figure 10 – The upper plot shows the variation of the wind speed in 10 minute intervals from Station 420421 in the Gulf of Mexico. The lower plot shows the slick ages predicted by the slick persistence model for this wind-speed history. Both plots are color coded for wind speed the same way with increasing wind speed from colder to hotter colors (see legend).

The slick age model shows significant annual variations in slick age with older slicks more common during the calmer summer months than the windier winter months (Fig. 10). These results are generally consistent with a study of seepage slicks from the Capsian Sea that analyzed both optical and SAR satellite imagery. It was found that the fraction of scenes with slicks was highest in the summer months (Mityagina and Lavrova, 2022). This was true for both optical and SAR imagery but was most pronounced for optical data that observed slicks at almost double the rate of SAR data in some months. Since optical imagery is not impacted by low wind speeds, the long slick persistence expected during lower wind speed months would be more fully captured in optical images than in SAR data which relies upon enough wind to create surface roughness for contrast.

Details of how the wind-speed history impacts slick age are easier to see contrast-

ing a winter month (February) with higher average wind speed with a summer month (July) with lower average wind speeds (Fig. 11). While both months show a similar range in wind speed, February has a much higher fraction of measurements above the 4 m/s speed at which breaking waves are generated.

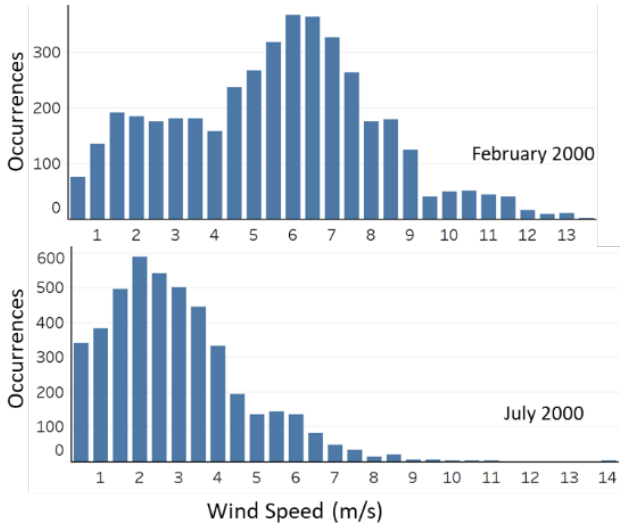

Figure 11 – Histograms of wind speed data (10 minutes intervals from Station 420421 in the Gulf of Mexico) for February and July 2000.

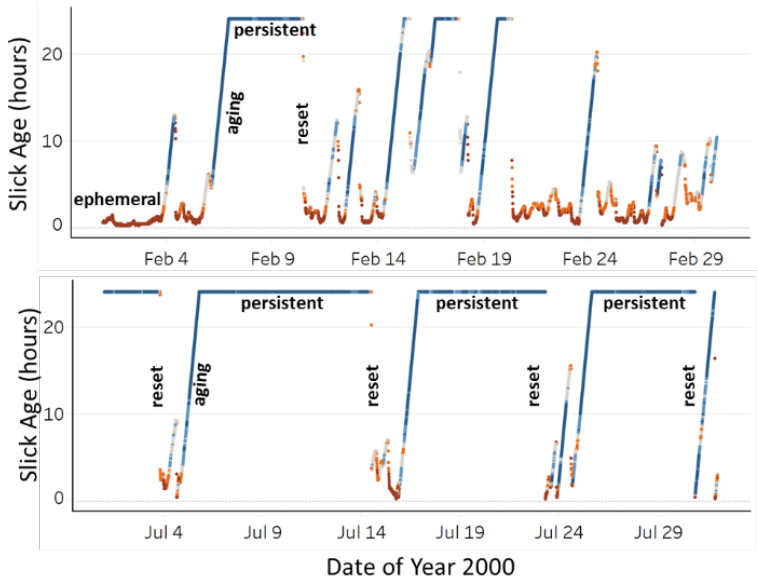

Figure 12 – Modeled slick ages as a function of time for February and July 2000

(10 minutes intervals from Station 420421 in the Gulf of Mexico).

The modeled slick ages for the two months are very different as expected from their wind-speed distributions; however, both months have the same four growth modes for slicks. These four modes are labeled for the slick age history (Fig. 12) and include:

1. persistent slicks – occur in extended periods of low wind speed
2. slick resets – a high wind speed event that disperses all slicks in an area
3. ephemeral slicks – occur in extended periods of high wind speed
4. aging slicks – the progressing growth of slicks following a reset

From February 1st to the 3rd, wind speeds are consistently high and ephemeral slicks are dispersed almost as fast as they are created. Wind speeds decrease around the 5th and aging slicks grow to the model limit of 24 hours by the 6th. From the 6th to the 10th low wind speeds allow slicks to persist whose size is not significantly governed by breaking waves. A reset occurs on the 10th dispersing the large slicks and leading to a period of alternating ephemeral and aging slicks. The same slick modes are seen in July but the difference in wind speeds between the months is manifest as much longer periods of persistent slicks in July than in February.

As an example of the importance of understanding slick longevity, consider slicks outlined from two SAR images over the same area in the Congo Basin, which are separated by 12 days from July 3rd and July 15th (Fig. 13). Sixteen OSOs were identified where slicks were detected in both images. Comparing the two images, the slicks on the 3rd are shorter and more uniform in length (2 – 6.3 km versus 2.5 – 26.1 km). As discussed earlier, slick length provides a useful way to estimate slick age as it is governed by the surface current speed, with some contribution from the wind. If one assumes uniform wind and current conditions, then differences in slick length are directly proportional to differences in slick ages. Considering the slicks from the 3rd, the relatively short and uniform lengths are consistent with a reset event having taken place prior to the scene capture and the slicks are in the aging mode. Alternatively, the short and uniform slick lengths could be explained by regional wind speeds of 5.5-7 m/s creating ephemeral slicks whose maximum ages are being limited by breaking waves. The slicks from the 15th vary in length by an order of magnitude. A relatively fast surface current velocity of 0.3 m/s would generate a 26 km long slick in ~ 24 hours and the shortest slicks from the 15th would be only 2 hours old if the current were uniform. The shorter slicks from the 15th have all drifted to the NW from their OSOs but the longer slicks drifted mostly to the W. We interpret these observations to indicate that the slicks are all in the aging mode transitioning to persistence. The difference in lengths is related to differences in currently velocities associated with either being closer to the core of an eddy (slower currents thus shorter slicks) or near it edge (faster currents thus longer slicks).

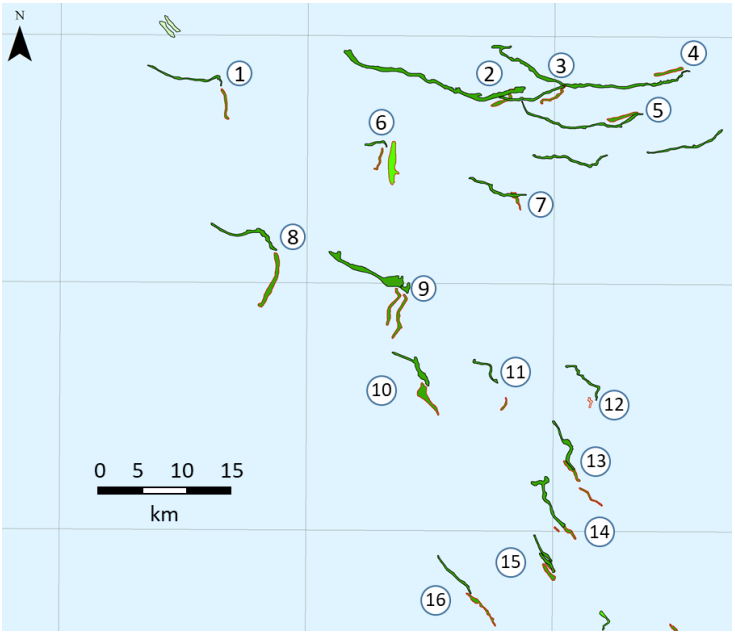

Figure 13 – Slick outlines derived from SAR images from the Congo Basin. Slicks with a red border are from July 3rd and those with a black border are from July 15th. Numbers indicate pairs of slicks from each day interpreted to be sourced from the same seepage point.

4.4 Slick Longevity and Oil Flux Estimates

Estimating the oil flux from natural seeps imaged by SAR satellites requires an estimate of slick thickness to convert the observed area to a volume and an estimate of the release time represented by the volume (the slick age; Meurer et al., 2022). Conversion of slick areas to volumes for natural slicks rely on an assumed thickness. Flux estimates differ in their approach to approximating an appropriate slick age. The hindcast approach examines individual slicks and uses regional wind and current data for each to match observed slick lengths with calculated lengths to estimate ages (Daneshgar-Asl et al., 2017). The more regional approach used by MacDonald et al. (2015) does not estimate individual seep fluxes but rather uses the fractional area covered by oil in satellite scenes to estimate fluxes. A range of slick ages from 8 to 24 hours were used to provide minimum and maximum flux estimates. Jatiault et al. (2017) examined seep fluxes in the Congo Basin using a somewhat intermediate approach. They examined individual slicks to estimate volumes for discrete seepage events and used the wind speed derived from the satellite images and a range of current velocities to estimate spreading speeds and thereby convert the slick lengths into ages. Similar to MacDonald et al. (2015), Jatiault et al. (2017) used the statistics of the current velocities to provide a range in ages and thus a minimum and maximum flux estimate.

The hindcast (Daneshgar-Asl et al., 2016) and current range (Jatiault et al., 2017) approaches both explicitly include the slick length in their estimation of the slick age and thereby oil flux per slick. This effectively takes into account the impact of the wind-speed history on the slicks so that reset events or persistent slicks are taken into account in flux estimates. The regional seepage method (MacDonald et al., 2015) requires a sufficiently large enough number of observations for an area that an average oil coverage can be defined and associated with an average age. The model for slick persistence based on the wind-speed history in the Gulf of Mexico (Fig. 10) yields an average slick persistence of 11.0 hours overall and 12.0 hours if time steps with winds <3 or >7 m/s are excluded (i.e., only weather compliant time steps). However, the distribution of slick ages is not normally distributed with persistent and ephemeral slicks dominating (Fig. 14). The model assumes a seep source that always releases enough oil to make a SAR imageable slick in 10 minutes (>10 ml/s for an image with a 25m pixel resolution). In contrast, most seeps in the Gulf of Mexico generate SAR observed slicks in less than 20% of observations with only a small fraction having a recurrence rate higher than 65% (O'Reilly et al., 2022; see Jatiault et al., 2017 for similar results from the Congo Basin).

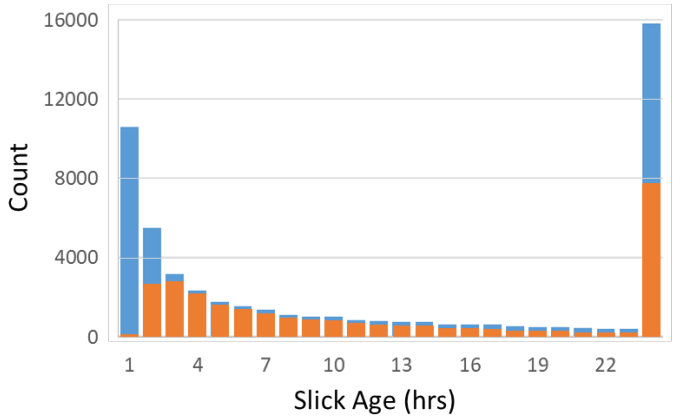

Figure 14 – Distribution of slick ages from Figure 8. The blue histogram in the back shows the distribution for all model times and the superposed orange histogram shows only time steps with wind speed between 3 and 7 m/s.

The implications for slick longevity suggested by different recurrence rates can be considered using a model based on oil column heights beneath capillary seals (Meurer et al., 2022; see also Leifer and Boles, 2005). We constructed a simple model that used four near surface traps that retain a fixed volume of oil before the column height generates enough pressure to overcome a capillary leak point. Once leakage begins the oil drains to the sea floor until the column height pressure is too low to maintain connectivity and the leak point is snapped off (Vassenden et al., 2003). The model release rates of oil from the traps are generally large enough to create SAR detectable slicks. The constant supply

of oil to the traps was varied to produce different slick recurrence rates (Fig. 15). The average slick longevity for a 65% recurrence rate model is 7.7 hours versus 5.5 hours for an 18% recurrence rate. The impact of oil release duration will impact persistent slicks preferentially because the average timing is much shorter than the age of persistent slicks (Fig. 14). These results indicate that variation in the seepage flux plays a significant role in determining slick longevity in the Gulf of Mexico. The combined effects of slick recurrence rates and wind speed suggest average slick longevities of less than 6.5 hours for seeps with high recurrence rates and less than 5 hours for those with recurrence rates less than ~25%. These results fit with the estimates of 6.4 hours slick longevity for GC600, a high slick recurrence seep (Daneshgar-Asl et al., 2016). The results also suggest that the upper flux estimate presented by MacDonald et al. (2015) based on an average slick age of 8 hours is up to ~35% too low and that a more appropriate age range for the oil on the surface would be 5 to 8 hours.

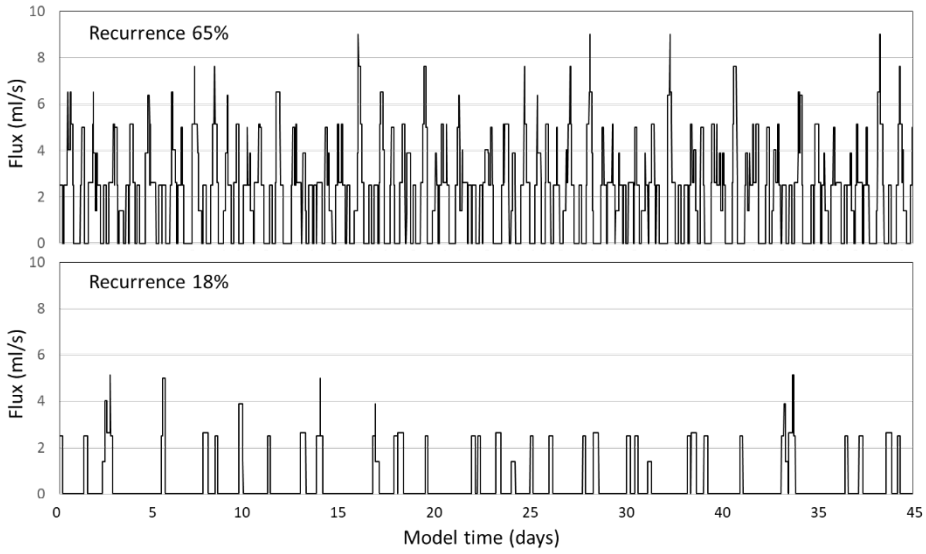

Figure 15 – Model results that simulate different slick histories for seeps with a slick recurrence rate of 65% and 18%. The vertical axis indicates the flux of oil reaching the sea surface as a function of time (the horizontal axis). The only difference between the models is the flux of oil into the system with the 65% recurrence model being supplied with oil at ~3 ml/s and the 18% recurrence model receiving only ~0.5 ml/s.

5 Conclusions

Comparison with experimental and field data suggest that both the oil ascent model and the slick longevity model can provide rapid insights into the fate of oil released from natural seeps. Both models have simplified inputs and algorithms making them suitable for Monte Carlo-type analysis. The oil ascent model pro-

vides a rapid tool for contrasting OSO offsets generated from oil-coated bubbles and oil droplets. These simulations could be used to test hypotheses for oil transport via bubbles or droplets at a given location. The model can also be used as a basis for defining the cluster size defined by slicks that are sourced from a single sea floor source. Simulations from seepage sites in differing water depths (600, 2500, 4000m) suggest greater OSO offset, as a function of water depth, for shallower sourced oil. These results are consistent with observations.

Slick longevity is found to be governed by both the wind-speed history and by the variability in flux from the seeps (which leads to intermittent slick recurrence). Modeling a year's worth of wind speed data for the Gulf of Mexico using the slick longevity model reveals four growth modes for seepage slicks: persistent (low wind speeds), ephemeral (high wind speeds), reset (all slicks are cleared from an area by high wind speeds), and aging (slick growth after a reset). Assuming a continuous oil supply, the results suggest an average slick age of ~ 12 hours. However, the distribution is not normal with the bulk of slicks being either ephemeral ($<$ 5 hours old) or persistent ($>$24 hours old). Modeled impact of intermittent seep flux on slick longevity for comparison suggests expected oil release duration implied by a 65% slick recurrence is ~7.7 hours while that for an 18% recurrence source is ~ 5.5 hours. These durations are longer than the longevity of ephemeral slicks but substantially shorter than that for persistent slicks. We estimate that combining effects of wind speed and flux variability will yield average slick longevities for high recurrence seeps of ~6.5 hours and ~ 5 hours for low recurrence seeps in the Gulf of Mexico.

Analysis of the impact of slick longevity on seep flux estimates demonstrates that methods that include the length of individual slicks and local currents and wind constraints are robust to the impact of wind-speed history and variable flux. However, approaches that assume an average slick age can be improved by incorporating the current findings.

Acknowledgments

W.P.M. and L.Z. are employed by the ExxonMobil Upstream Research Company. The findings of this research have no bearing on any financial or public relation concerns of ExxonMobil Corporation. This work was funded, in part, by a grant from ExxonMobil Upstream Research Company to Ian MacDonald and Florida State University. W.P.M. and L.Z. thank colleagues for support and ideas that contributed to this work. They also thank ExxonMobil Upstream Research Company for support of this work and for agreeing to release the findings.

Open Research

All data used in this study are derived from other published and/or publically available sources and are referenced in the text.

References

Allen, A.A., Schueter, R.S., & Mikoalaj, P.G. (1970) Natural Oil Seepage at Coal Oil Point, Santa Barbara, California, *Science*, 170, 974-977.

Aeppli, C., Mitchell, D.A., Keyes, P., Beirne, E.C., McFarlin, K.M., Roman-Hubers, A.T., Rusyn, I., Prince, R.C., Zhao, L., Parkerton, T.F. & Nedwed, T. (2022) Oil Irradiation Experiments Document Changes in Oil Properties, Molecular Composition, and Dispersant Effectiveness Associated with Oil Photo-Oxidation, *Environmental Science & Technology*, 56(12), 7789-7799.

Bleck, R. (2002) An oceanic general circulation model framed in hybrid isopycnic-Cartesian coordinates, *Ocean Model*, 4, 55-88.

Brekke, C., Espeseth, M.M., Dagestad, K.-F., Röhrs, J., Hole, L.R., & Reigber, A.(2021) Integrated Analysis of Multisensor Datasets and Oil Drift Simulations - A Free-Floating Oil Experiment in the Open Ocean, *J.Geophys. Res. Oceans*, 126, doi.org/10.1029/2020JC016499

Callaghan, A., de Leeuw, G., Cohen, L. & O'Dowd, C.D. (2008) Relationship of oceanic whitecap coverage to wind speed and wind history, *Geophys. Res. Let.*, 35, L23609, doi:10.1029/2008GL036165

Callaghan, A.H., Deane, G.B., Stokes, M.D., and Ward, B. (2012) Observed variation in the decay time of oceanic whitecap foam, *J. Geophys. Res.*; 117, C09015, doi:10.1029/2012JC008147

Clift, R., Grace, J. R., & Weber, M. E. (1978) *Bubbles, Drops, and Particles*. New York, NY: Academic Press.

Daneshgar-Asl, S., Dukhovskoyb, D.S., Bourassa, M., & MacDonald, I.R. (2017) Hindcast modeling of oil slick persistence from natural seeps, *Remote Sensing of Environment*, 189, 96–107, doi:10.1016/j.rse.2016.11.003

De Dominicis, M., Bruciaferri, D., Gerin, R., N.Pinardi, N., Poulain, P.M., Garreau, P., Zodiatis, G., Perivoliotis, L., Fazioli, L., Sorgente, R., & Manganiello, C. (2016) A multi-model assessment of the impact of currents, waves and wind in modelling surface drifters and oil spill, *Deep Sea Research Part II: Topical Studies in Oceanography*, 133, 21-38, doi.org/10.1016/j.dsr2.2016.04.002

Dissanayake, A.L., Gros, J. & Socolofsky, S.A. (2018) Integral models for bubble, droplet, and multiphase plume dynamics in stratification and crossflow. *Environ Fluid Mech.*, 18, 1167–1202. doi.org/10.1007/s10652-018-9591-y

Fay, J. (1969) The Spread of Oil Slicks on a Calm Sea, in *Oil on the Sea*; Hoult, D.P., Ed.; Springer: Boston, MA, USA, pp. 53–63.

Garcia-Pineda, O., MacDonald, I., Zimmer, B., Shedd, B., & Roberts, H. (2010) Remote-sensing evaluation of geophysical anomaly sites in the outer continental slope, northern Gulf of Mexico, *Deep Sea Research Part II: Topical Studies in Oceanography*, 57,1859-1869. doi.org/10.1016/j.dsr2.2010.05.005

Garcia-Pineda, O., MacDonald, I., Silva, M., Shedd, W., Daneshgar Asl, S., & Schumaker, B. (2016) Transience and persistence of natural hydrocarbon

seepage in Mississippi Canyon, Gulf of Mexico, *Deep Sea Research Part II: Topical Studies in Oceanography*, 129, 119-129.

Geng, X., Boufadel, M.C., Ozgokmen, T., King, T., Lee, K., Lu, Y., & Zhao, L. (2016) Oil droplets transport due to irregular waves: Development of large-scale spreading coefficients. *Mar. Pollut. Bull.*, 104, 279–289.

Goncharov, K. (2009) Simulation of oil drops dynamics in seawater environment, *J. Med. Eng. Technol.,* 8, 21–28.

Grace, J.R. & TH, N. (1976) *Shapes and velocities of single drops and bubbles moving freely through immiscible liquids*.

Greinert, J., Artemov, Y., Egorov, V., De Batist, M., & McGinnis, D. (2006), 1300-m-high rising bubbles from mud volcanoes at 2080m in the Black Sea: Hydroacoustic characteristics and temporal variability, *Earth Planet. Sci. Lett.*, 244(1), 1–15.

Gros, J., Arey, J.S., Socolofsky, S.A., & Dissanayake, A. L. (2020) Dynamics of Live Oil Droplets and Natural Gas Bubbles in Deep Water, *Environmental Science & Technology*, 54, 11865-11875, DOI:10.1021/acs.est.9b06242

Gros, J., Socolofsky, S.A., Dissanayake, A.L., Jun, I., Zhao, L., Boufadel, M.C., Reddy, C.M. & Arey, J.S. (2017) Petroleum dynamics in the sea and influence of subsea dispersant injection during Deepwater Horizon, *Proceedings of the National Academy of Sciences*, 114(38), 10065-10070.

Haberman, W.L. & Morton, R.K. (1956) An experimental study of bubbles moving in liquids, *Transactions of the American Society of Civil Engineers*, 121(1), pp.227-250.

Holstein, A., Kappas, M., · Propastin, P., & Renchin, T. (2018) Oil spill detection in the Kazakhstan sector of the Caspian Sea with the help of ENVISAT ASAR data, *Environmental Earth Sciences*, 77, 198, doi.org/10.1007/s12665-018-7347-0

Jaggi, A., Snowdon, R.W., Stopford, A., Radović, R.J., Oldenburg, T.B.P., & Larter, S.R. (2017) Experimental simulation of crude oil-water partitioning behavior of BTEX compounds during a deep submarine oil spill, *Organic Geochemistry*, 108, 1-8. doi.org/10.1016/j.orggeochem.2017.03.006

Jatiault, R., Dhont, D., Loncke, L., & Dubucq, D. (2017) Monitoring of natural oil seepage in the Lower Congo Basin using SAR observations, *Remote Sensing of Environment*, 191, 258-272. doi.org/10.1016/j.rse.2017.01.031

Jatiault, R., Dhont, D., Loncke, L., de Madron, X.D., Dubucq, D., Channelliere, C., & Bourrin, F. (2018) Deflection of natural oil droplets through the water column in deep-water environments: The case of the Lower Congo Basin, *Deep Sea Research Part I: Oceanographic Research Papers*, 136, 44-61, doi.org/10.1016/j.dsr.2018.04.009

Jenkins, A.D. & Jacobs, S.J. (1977) Wave damping by a thin layer of viscous fluid, *Phys. Fluids*, 9, 1256-1264.

Johansen, C., Todd, A.C., & MacDonald, I.R. (2017) Time series video analysis of bubble release processes at natural hydrocarbon seeps in the northern Gulf of Mexico, *Mar. Pet. Geol.*, 82, 21-34.

Lehr, W., Jones, R., Evans, M., Simecek-Beatty, D., & Overstreet, R. (2002) Revisions of the ADIOS oil spill model. *Environ. Model. Softw.*, 17, 189–197.

Lehr, W., & Socolofsky, S.A. (2020) The Importance of Understanding Fundamental Physics and Chemistry of Deep Oil Blowouts. In Deep Oil Spills; Springer: Cham, Switzerland, pp. 14–24.

Leifer, I & Boles, J (2005) Measurement of marine hydrocarbon seep flow through fractured rock and unconsolidated sediment, *Marine and Petroleum Geology*, 22, :551-568, doi.org/10.1016/j.marpetgeo.2004.10.026.

Li, H., Bao, M., Li, Y., Zhao, L., King, T., & Xie, Y. (2020) Effects of suspended particulate matter, surface oil layer thickness and surfactants on the formation and transport of oil-sediment aggregates (OSA). *Int. Biodeterior. Biodegrad.*, 149, 104925.

Keramea P, Spanoudaki K, Zodiatis G, Gikas G, Sylaios G. (2021) Oil Spill Modeling: A Critical Review on Current Trends, Perspectives, and Challenges, *Journal of Marine Science and Engineering*, 9(2),181. doi.org/10.3390/jmse9020181

MacDonald, I.R., Guinasso Jr., N.L., Ackleson, S.G., Amos, J.F., Duckworth, R., Sassen, R., & Brooks, J.M. (1993) Natural Oil Slicks in the Gulf of Mexico Visible From Space, *J. Geophys Res.*, 98, 16,351-16,364.

MacDonald, I. R., Garcia-Pineda, O., Beet, A., Daneshgar Asl, S., Feng, L., Graettinger, G., French-McCay, D., Holmes, J., Hu, C., Huffer, F., Leifer, I., Muller-Karger, F., Solow, A., Silva, M., & Swayze, G. (2015) Natural and unnatural oil slicks in the Gulf of Mexico, *Journal Geophys. Res. Oceans*, 120, 8364-8380. doi.org/10.1002/2015JC011062

Mackay, D., Buist, I.A., Mascarenhas, R., & Paterson, S. (1980) *Oil Spill Processes and Models: Environment Canada Manuscript Report No 8*; Environment Canada: Ottawa, ON, Canada.

Maini, B. B., & Bishnoi, P. (1981), Experimental investigation of hydrate formation behaviour of a natural gas bubble in a simulated deep sea environment, *Chem. Eng. Sci.*, 36(1), 183–189.

McCain, W.D. (1991) Reservoir-fluid property correlations—state of the art, *SPE Reservoir Engineering*, 6(02), 266-272.

Meurer, W.P., Blum, J., & Shipman, G. (2021) Volumetric Mapping of Methane Concentrations at the Bush Hill Hydrocarbon Seep, Gulf of Mexico, *Front. Earth Sci.*, 27, doi.org/10.3389/feart.2021.604930

Meurer, W.P., Daneshgar Asl, S., O'Reilly, C., Silva, M., & MacDonald, I.R. (2022) Quantitative estimates of oil-seepage rates from satellite imagery with implications for oil generation and migration rates, submitted to EPSL

Mityagina, M., & Lavrova, O. (2022) Satellite Survey of Offshore Oil Seep Sites in the Caspian Sea. *Remote Sens.*, 14, 525. doi.org/10.3390/rs14030525

Motarjemi, M., & Jameson, G. (1978), Mass transfer from very small bubbles: The optimum bubble size for aeration, *Chem. Eng. Sci.*, 33(11), 1415–1423.

Najoui, Z., Riazanoff, S., Deffontaines, B., & Xavier, J.P. (2018) Estimated location of the seafloor sources of marine natural oil seeps from sea surface outbreaks: A new "source path procedure" applied to the northern Gulf of Mexico, *Marin and Petroleum Geology*, 91, 190-201. doi.org/10.1016/j.marpetgeo.2017.12.035

O'Reilly, C., Silva, M., Daneshgar Asl, S., Meurer, W.P., & MacDonald, I.R. (2022) Distribution, Magnitude, and Variability of Natural Oil Seeps in the Gulf of Mexico, *Remote Sens.*, 14, 3150, doi.org/10.3390/rs14133150

Pesch, S., Schlüter, M., Aman, Z.M., Malone, K., Krause, D., & Paris, C.B. (2020) Behavior of Rising Droplets and Bubbles: Impact on the Physics of Deep-Sea Blowouts and Oil Fate, in *Deep Oil Spills*; Springer: Cham, Switzerland; pp. 65–82.

Phillips, O.M. (1985) Spectral and statistical properties of the equilibrium range in wind-generated gravity waves, *J. Fluid Mech.*, 156, 505-531.

Razaz, M., Di Iorio, D.,Wang, B., Daneshgar Asl, S., & Thurnherr, A. M. (2020) Variability of a Natural Hydrocarbon Seep and its Connection to the Ocean Surface. *Nature Sci. Rep.,* 10, 12654. doi:10.1038/s41598-020-68807-4

Rehder G., Brewer P.G., Peltzer E.T., & Friederich G. (2002) Enhanced lifetime of methane bubble streams within the deep ocean, *Geophys. Res. Lett.*, 29, 21-1:4, 10.1029/2001GL013966

Rehder, G., Leifer, I., Brewer, P.G., Friederich, G., & Peltzer, E.T. (2009) Controls on methane bubble dissolution inside and outside the hydrate stability field from open ocean field experiments and numerical modeling, *Marine Chemistry*, 114, 19-30. doi.org/10.1016/j.marchem.2009.03.004

Romano, J.-C. (1996) Sea-surface slick occurrence in the open sea (Mediterranean, Red Sea, Indian Ocean) in relation to wind speed, *Deep Sea Research*, 43, 411-423.

Römer, M., Hsu, C.-W., Loher, M., MacDonald, I.R., Ferreira, C.d.S., Pape, T., Mau, S., Bohrmann, G., & Sahling, H. (2019) Amount and Fate of Gas and Oil Discharged at 3400 m Water Depth From a Natural Seep Site in the Southern Gulf of Mexico, *Front. Mar. Sci.*, doi.org/10.3389/fmars.2019.00700

Sergievskaya, I.A. & Ermakov, S.A. (2017) Damping of Gravity–Capillary Waves on Water Surface Covered with a Visco-Elastic Film of Finite Thickness, Izvestiya, *Atmospheric and Oceanic Physics*, 53, 650-658.

Sim, L., Graham, J., Rose, K., Duran, R., Nelson, J., Umhoefer, J., & Vielma, J. (2015) *Developing a Comprehensive Deepwater Blowout and Spill Model*; U.S. Department of Energy, National Energy Technology Laboratory: Albany, NY, USA, p. 44.

Simecek-Beatty, D. & Lehr, W.J. (2017) Extended oil spill spreading with Langmuir circulation, *Marine Pollution Bull.*, 122, 226-235. doi.org/10.1016/j.marpolbul.2017.06.047

Socolofsky, S.A., Adams, E.E., Boufadel, M.C., Aman, Z.M., Johansen, Ø., Konkel, W.J., Lindo, D., Madsen, M.N., North, E. W., Paris, C.B., Rasmussen, D., Reed, M., Rønningen, P., Sim, L. H., Uhrenholdt, T., Anderson, K.G., Cooper, C., & Nedwed, T.J. (2015) Intercomparison of oil spill prediction models for accidental blowout scenarios with and without subsea chemical dispersant injection, *Marine Pollution Bulletin*, 96, 110-126, doi.org/10.1016/j.marpolbul.2015.05.039

Tkalich, P., & Chan, E.S (2002) Vertical mixing of oil droplets by breaking waves, *Marine Pollution Bull.*, 44, 1219-1229. doi.org/10.1016/S0025-326X(02)00178-9

Tsuchiya, K., Mikasa, H. & Saito, T., (1997) Absorption dynamics of CO2 bubbles in a pressurized liquid flowing downward and its simulation in seawater. *Chemical Engineering Science*, 52(21-22), 4119-4126.

Vassenden, F., Sylta, Ø., & Zwach, C. (2003) Secondary Migration in a 2D Visual Laboratory Model, Conference Proceedings, *First EAGE International Conference on Fault and Top Seals - What do we know and where do we go?*, Sep 2003, cp-97-00004, Pub. European Association of Geoscientists & Engineers, doi.org/10.3997/2214-4609.201405814

Wang, D.T., Meurer, W.P., Nguyen, T.N., Shipman, G.W., & Koenig, D. (2021) Preservation of oil slick samples on adsorbent Teflon fabric: Potential for deployment aboard autonomous surface vessels, *Marine Pollution Bull.*, 169, 112460. doi.org/10.1016/j.marpolbul.2021.112460

Wei, L., Jie, P.Y., Guo, L.J., & Xiao, L. (2009) Computational modeling of submarine oil spill with current and wave by FLUENT, *Research Journal of Applied Sciences, Engineering and Technology*, .5, 5077-5082.

Xue, J., Yu, Y., Bai, Y., Wang, L., & Wu, Y. (2015) Marine oil-degrading microorganisms and biodegradation process of petroleum hydrocarbon in marine environments: A review. *Curr. Microbiol.*, 71, 220–228.

Yapa, P.D., Wimalaratne, M.R., Dissanayake, A.L., & DeGraff, J.A., Jr. (2012) How does oil and gas behave when released in deepwater? *J. Hydro Environ. Res.*, 6, 275–285.

Zatsepa, S. N., Ivchenkoa, A. A., Korotenkob, K. A., V. V. Solbakova, c, & V. V. Stanovoyd (2018) Phenomenological Model of Natural Dispersion of an Oil Spill in the Sea and Some Associated Parameterization Processes, *Oceanology*, 58, 769–777, doi:10.1134/S0001437018060152

Zhao, L., Boufadel, M.C., Socolofsky, S.A., Adams, E., King, T. & Lee, K. (2014) Evolution of droplets in subsea oil and gas blowouts: Development and validation of the numerical model VDROP-J. *Marine Pollution Bulletin*, 83(1), 58-69.

Zhao, L., Boufadel, M.C., Lee, K., King, T., Loney, N. & Geng, X. (2016) Evolution of bubble size distribution from gas blowout in shallow water. *Journal of Geophysical Research: Oceans*, 121(3), 1573-1599.

Zhao, L., Nedwed, T., Daling, P.S. & Brandvik, P.J. (2022) Investigation of the spreading tendency of emulsified oil slicks on open systems. *Marine Pollution Bulletin*, 180, 113739.

Zheng, L. & Yapa, P.D. (2000) Buoyant velocity of spherical and nonspherical bubbles/droplets. *Journal of Hydraulic Engineering*, 126(11), 852-854.